Heliyon 9 (2023) e17693

Contents lists available at ScienceDirect

Heliyon

journal homepage: www.cell.com/heliyon

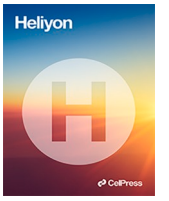

Fiberglass cloth coated by coffee ground waste-derived carbon quantum dots/titanium dioxide composite for removal of caffeine and other pharmaceuticals from water

Rattana Muangmora [a], Patiya Kemacheevakul [a,b,c,*], Surawut Chuangchote [b,d]

[a] Department of Environmental Engineering, Faculty of Engineering, King Mongkut's University of Technology Thonburi, 126 Prachauthit Rd., Bangmod, Thungkru, Bangkok 10140, Thailand
[b] Research Center of Advanced Materials for Energy and Environmental Technology (MEET), King Mongkut's University of Technology Thonburi, 126 Prachauthit Rd., Bangmod, Thungkru, Bangkok 10140, Thailand
[c] Center of Excellence on Hazardous Substance Management (HSM), Bangkok 10330, Thailand
[d] Department of Tool and Materials Engineering, Faculty of Engineering, King Mongkut's University of Technology Thonburi, 126 Prachauthit Rd., Bangmod, Thungkru, Bangkok 10140, Thailand

ARTICLE INFO

Keywords:
Coffee ground waste
Carbon quantum dots
Caffeine
Titanium dioxide
Fiberglass cloth
Visible-light photocatalysis

ABSTRACT

Coffee ground waste from the coffee beverage preparation is mainly discarded and consequently ends up in landfill, which cause the contamination of caffeine in various environmental compartments. This study focuses on the upcycling of coffee-ground waste to carbon quantum dots (CQDs) for use as a modifying material to improve the visible light activity of titanium dioxide (TiO_2). The CQD solution was synthesized by hydrothermal method, which has an average size of 2.80 ± 0.63 nm. The CQDs/TiO_2 photocatalysts were prepared by combining CQD solutions at various amounts with sol-gel TiO_2 and then coated on the fiberglass cloths (FGCs). The photocatalytic application mainly focuses on the removal of caffeine from the water. The photocatalytic experiment was preliminary run in a simple batch reactor under visible light. The 5CQDs/TiO_2 coated FGC (5 mL of CQD solution/g of Ti-based on sol-gel) showed the best performance, and it was selected for the removal of caffeine and other pharmaceuticals (i.e., carbamazepine and ibuprofen) in the recirculating reactor. The removals of caffeine, carbamazepine, and ibuprofen after irradiation for 9 h were 82%, 88%, and 84%, respectively. The residual concentrations were significantly lower than the reported toxicity levels based on specific species. The changes in total organic carbon were observed, indicating the mineralization of pharmaceuticals in water. The 5CQDs/TiO_2 coated FGC showed good flexible performance. No obvious loss of activity was observed for five runs. The actual wastewater from the coffee pot cleaning process was also tested. The removal was 80% for caffeine and 86% for color in the unit of the American Dye Manufacturers Institute (ADMI).

1. Introduction

Coffee is one of the most popular beverages, with a worldwide consumption rate of 2.25 billion cups per day [1]. Coffee beverage

* Corresponding author. Department of Environmental Engineering, Faculty of Engineering, King Mongkut's University of Technology Thonburi, 126 Prachauthit Rd., Bangmod, Thungkru, Bangkok 10140, Thailand.
E-mail address: patiya.kem@kmutt.ac.th (P. Kemacheevakul).

https://doi.org/10.1016/j.heliyon.2023.e17693
Received 12 June 2023; Received in revised form 23 June 2023; Accepted 26 June 2023
Available online 28 June 2023

preparation, especially coffee brewing at home, in cafeterias, and in manufacturing industries, generates much coffee ground waste. The worldwide production of coffee ground waste is approximately 6–8 million tons annually [2], mainly in landfill sites [3].

CAF is a dominant constituent in coffee ground waste, which is hazardous to the environment [4]. Disposing of coffee ground waste in a landfill may cause CAF-containing leachate to flow through the soil and groundwater [5]. The recycling of coffee ground waste is a practical approach to reducing the environmental impact and also saving disposal costs. The current strategies for recycling coffee ground waste mainly involve upgrading to adsorbent and biofuel because it contains high organic content [3].

CAF, CBZ, and IBP are frequently detected in the same water bodies because of their enormous consumption. Besides coffee, there are many caffeinated food, beverages, and medicines (e.g., cold medicines, analgesics, and weight-loss drugs) worldwide [6]. CBZ and IBP have been listed in the Model List of Essential Medicines 2019 by World Health Organization (WHO) as anticonvulsant and non-steroidal anti-inflammatory drugs (NSAIDs), respectively [7]. The observed concentrations of pharmaceuticals in their manufacturing wastewater were 0.022–3.594 mg/L for CAF [8], 0.077–0.575 mg/L for CBZ [9], and 0.703–1.673 mg/L for IBP [10]. These concentrations significantly exceed the lowest observed effect concentration (LOEC), which has been reported in chronic toxicity studies for specific organisms such as fish (0.91 mg/L CAF) [6], water fleas (0.1 mg/L CBZ) [11], and diatoms (1 mg/L IBP) [12].

A large portion of pharmaceutical wastewater originates from the manufacturing process in the pharmaceutical industry [13]. The pharmaceutical industry in many areas still discharges untreated effluents into the sewers [9]. Most pharmaceuticals are resistant to sewage treatment plants because of their low biodegradability and high solubility in water [14], so they could eventually contaminate the aquatic environment. Consequently, it is reasonable to apply advanced technology for the treatment of pharmaceuticals in water to minimize toxicological risk to the ecosystem.

Semiconductor photocatalysis is one of the promising options for the advanced treatment of refractory organic compounds such as pharmaceuticals in water [15]. This technology is a cost-effective approach because it can harvest solar energy, does not require external oxidants (e.g., ozone, hydrogen peroxide), does not require waste disposal (e.g., sludge disposal), and allows high reusability of the photocatalyst film without complex processes [16,17]. Titanium dioxide (TiO_2) has been reported as an efficient photocatalyst for both fundamental research and practical applications. However, there are some limitations of TiO_2, including (i) the intrinsic wide band gap of TiO_2 (3.2 eV for anatase), which limits its application under visible light, and (ii) the rapid recombination of photo-excited electrons and holes, which lead to the decrease of its photocatalytic activity [18].

CQDs are a new class of fluorescent carbon nanomaterials with a size below 10 nm [19,20]. CQDs have received much attention because of their attractive properties, such as good water solubility, large specific surface area, low toxicity, and excellent photoluminescence behavior [19]. CQDs can be applied in many fields, such as bio-imaging, sensing, drug delivery, and photocatalysis [21]. CQDs have been used as modifying materials to improve visible light harvesting of TiO_2 photocatalysts. In the previous studies on CQDs/TiO_2, the CQDs were usually synthesized from chemical precursors such as citric acid [20,22], sodium citrate [23], and L-ascorbic acid [24], and in most studies, the CQDs/TiO_2 powder was dispersed in wastewater as a photocatalyst.

Food waste is a cost-effective raw material for the synthesis of CQDs. In recent years, CQDs have been successfully synthesized using different kinds of food waste, such as coffee ground waste [25–27], onion peel [28], crab shells [29], and tea waste [30]. Some researchers have already used coffee ground waste as a starting material for synthesizing CQDs during 2016–2022. The obtained CQDs were efficiently used for bio-imaging [25], detection of heavy metals including Fe^{3+} and Cu^{2+} [25,26], and detection of noxious nitroanilines [27]. However, these previous studies did not investigate the potentiality of coffee ground waste-derived CQDs for other applications such as photocatalysis.

This study presents an alternative way to take advantage of the coffee ground waste-derived CQDs. The CQDs were used to modify the visible light activity of TiO_2. The objectives of this study are to upcycle the coffee ground waste as CQDs and develop a visible light-active photocatalyst using coffee ground waste-derived CQDs composite with TiO_2 for the removal of pharmaceuticals from water. The CQDs were combined with sol-gel TiO_2 and coated on the FGC to overcome the difficulty in catalyst separation and recovery at the end of the photocatalytic process. CAF was the primary target pollutant to investigate the visible-light activity of FGC coated with CQDs/TiO_2 in a simple batch reactor and recirculating reactor. The optimum photocatalyst was also applied to remove other pharmaceuticals, including CBZ and IBP, and to remove CAF from the actual wastewater generated from the coffee-pot cleaning process. The reusable and flexible photocatalysts which are beneficial for practical applications were investigated and reported.

2. Materials and methods

2.1. Materials and chemicals

Ultrapure water from the water purification system (Millipore, resistivity of 18.2 mΩ cm) was used in all preparations and experiments. The coffee ground waste (Arabica, average moisture content of 36.8 ± 3.2%) was dried at 105 °C for 24 h before use for the synthesis of CQD solution. FGC (C-glass type, HT800) was supplied by Zaftec company, Thailand. Commercial TiO_2 powder (pure anatase, 98.5%), acetylacetone (ACAC, ≥99.5%), hydrogen peroxide solution (H_2O_2, 30% w/v), dipotassium phosphate (K_2HPO_4, ≥98%) and potassium dihydrogen phosphate (KH_2PO_4, 99%) were purchased from Carlo Erba Reagents. Tetrabutyl titanate (TBOT, 97%), CAF (99%), CBZ (98%), and IBP (98%) were purchased from Sigma-Aldrich. Sodium hydroxide pellets (NaOH, 99%) were purchased from QRëC. Methanol (HPLC grade), water (HPLC grade), acetonitrile (HPLC grade), and dichloromethane (99.8%) were purchased from RCI Labscan.

2.2. Synthesis and characterizations of CQD solutions

CQDs were synthesized by the one-pot hydrothermal method. NaOH (3.2 g) was stirred with ultrapure water (400 mL) for 10 min. The dried coffee ground waste (15 g) was dispersed in NaOH solution under constant stirring for 1 h H_2O_2 (100 mL) was slowly added to the mixture and manually stirred using a glass rod. The obtained mixture was heated at 300 °C for 4 h in a 500-mL hydrothermal reactor equipped with 4848 reactor controllers (Parr instrument company, USA). After cooling to room temperature, the solid part was separated using 6 μm and 0.2 μm filter papers, while the liquid part was then purified by dichloromethane three times. The purified CQD solutions were characterized using a transmission electron microscope (TEM, JEOL model JEM 2100) and a photoluminescence spectrometer (HORIBA Scientific, model: FLUOROMAX-4). The CQDs concentration in the solution was measured as total carbon in triplicate using a total organic carbon (TOC) analyzer (Analytik Jena, Multi N/C 3100). The average total carbon in CQD solution was 5.72 mg/mL.

2.3. Preparation of CQDs/TiO_2 powders and CQDs/TiO_2 coated FGC

CQDs/TiO_2 was prepared by ultrasonic-assisted sol-gel method. Firstly, a mixture of TBOT (8 g), ACAC (2.35 g), and methanol (40 mL) was magnetically stirred for 30 min. After that, a certain volume of CQD solutions (1, 2, 3, 4, 5, 6, 9, or 12 mL/g of Ti) was dropped into the mixture under stirring for another 30 min. The obtained mixture was sonicated in an ultrasonic bath (Crest, 690HTAE) for 30 min and aged for 24 h. The reference TiO_2 (without CQDs) was also prepared by this procedure without the addition of any CQD solution. For the preparation of CQDs/TiO_2 powder, sol-gel CQDs/TiO_2 was dried at 105 °C for 24 h, milled and sieved with mesh (No. 200), and finally calcined at 500 °C for 1 h under N_2 gas.

For the preparation of CQDs/TiO_2 coated FGC, the FGC pieces were heated at 500 °C for 1 h (heating rate of 10 °C/min) to eliminate the organic compounds on their surface. There are two coating steps as follows: (i) the FGC pieces were firstly coated by a mixture of commercial anatase TiO_2 powder and ultrapure water (2 g/L) using a paintbrush, followed by drying for 1 h (105 °C) and calcined in the air for 2 h (200 °C, heating rate of 2 °C/min), and (ii) the sol-gel-derived CQDs/TiO_2 was gently dropped over the prior layer followed by drying at room temperature for 24 h, dried in the oven for 1 h (105 °C), and finally calcined under 1 mL/min nitrogen gas for 1 h (500 °C, heating rate of 10 °C/min). In each step, the TiO_2 mixture was coated on FGC with a fixed ratio of 0.06 mL/cm^2. The obtained photocatalysts were labeled as FGC coated with xCQDs-TiO_2 (x = mL of CQD solution/g of Ti-based on sol-gel).

2.4. Characterizations of photocatalysts

The as-synthesized CQDs/TiO_2 powders without coating on FGC were characterized by X-ray diffractometer (XRD, BRUKER AXS, D8DISCOVER), Fourier transform infrared spectroscopy (FTIR, Thermo, Nicolet 6700), and photoluminescence spectrometer (HORIBA Scientific, model: FLUOROMAX-4) to avoid the noise of FGC as recommended in previous studies [31,32]. The surface morphology of the FGCs coated with CQDs/TiO_2 was investigated using a field emission scanning electron microscope (FESEM, model: NOVA NANOSEM 450). The absorption and reflection spectra were measured using a UV-VIS-NIR spectrophotometer (Shimadzu SolidSpec-3700) to determine the band gap energy using the Kubelka-Munk equation and the Tauc plot method [33].

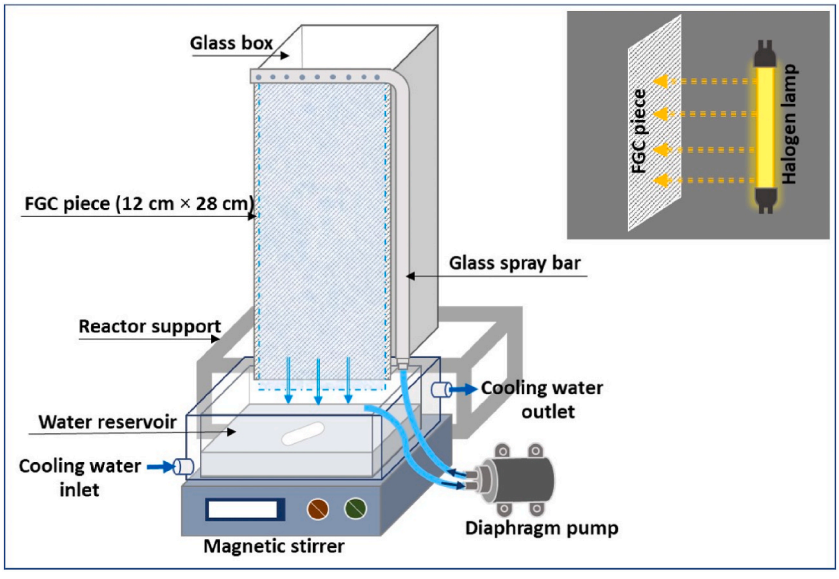

Fig. 1. A recirculating reactor with an inset showing the direction of visible light irradiation.

2.5. Photocatalytic experiments

For all experiments, the reactions were initially carried out for 3 h in the dark to ensure the adsorption/desorption equilibrium. Then the visible light was irradiated by a double-ended halogen lamp (Philips, Plusline, R7s, 300W). The distance of the light source from the surface of FGC was fixed at 25 cm. CAF was the main target pollutant for the photocatalytic experiment. Fundamentally, the wastewater temperature directly affects the degradation rate of organic pollutants in water and solvent evaporation. Therefore, it was controlled at around 28.5 ± 1.5 °C using a water-cooling system throughout the experiments.

Firstly, the optimization of CQDs content in sol-gel CQDs/TiO_2 was studied in a simple batch reactor through photocatalytic degradation of CAF. A piece of photocatalyst-coated FGC (10 cm × 10 cm) was soaked in pharmaceutical solution (60 mL) inside a glass container (10 cm × 10 cm × 6 cm) under horizontal shaking (60 rpm).

The optimal photocatalyst-coated FGC was obtained and further used in the recirculating reactor (Fig. 1) to remove CAF and other pharmaceuticals (i.e., CBZ and IBP) at the concentrations found in their production effluents [8–10]. The photocatalysis experiments were performed by stretching a piece of FGC coated with optimum photocatalyst (12 cm × 28 cm) through the surface of a glass box. The wastewater was pumped into a glass spray bar and subsequently ran down to the water reservoir by gravity. The solution was recirculated at a 450 mL/min flow rate using a diaphragm pump. Magnetic stirring was performed throughout the experiments to ensure that the solution was completely mixed. At desired reaction intervals, 1 mL of samples were taken and filtrated with a 0.22 μm nylon syringe filter. The influences of irradiation time and initial concentration of pharmaceuticals on the removal of CAF, CBZ, and IBP were investigated. The reuse and regeneration of the photocatalyst-coated FGC were also investigated for five cycles through the photocatalytic degradation of CAF. The removal of CAF from actual wastewater was investigated using wastewater collected from the coffee-pot cleaning process.

2.6. Analytical procedures

The quantification of pharmaceuticals in water was performed by high-performance liquid chromatography (HPLC) using the Alliance-e2695 Separations Module. A stationary phase was a C18-column (Vertisep™, 4.6 mm × 150 mm, particle size of 5 μm) with a column temperature of 30 °C. The mobile phases consisted of methanol and ultrapure water (50:50 v/v, flow rate = 1 mL/min) for CAF, acetonitrile, and ultrapure water (60:40 v/v, flow rate = 1 mL/min), and 20 mM phosphate buffer (pH = 7.4) and acetonitrile (70:30 v/v, flow rate = 1.2 mL/min). The injection volume of each sample was set at 100 μL. CAF and CBZ were detected by a photodiode array detector (Waters 2998) at 280 nm for CAF and 285 nm for CBZ. IBP was detected by a fluorescent detector (FP-2020, JASCO) at the excitation and emission wavelengths of 263 nm and 288 nm, respectively. Besides HPLC measurements, the mineralization of pharmaceuticals in water was also estimated using a total organic carbon (TOC) analyzer (Analytik Jena, Multi N/C 3100). NPOC method was used for TOC measurement with the sample volume of 500 mL and the furnace temperature of 800 °C. The color of wastewater was measured in the unit of the American Dye Manufacturers Institute (ADMI) using a UV-VIS spectrophotometer (Hach, DR6000).

3. Results and discussion

3.1. Properties of CQD solutions

The morphology of coffee ground waste-derived CQDs was characterized by TEM. The representative TEM image is shown in Fig. 2a. CQDs are spherical and mono-dispersed in the as-prepared solution. The inset of Fig. 2a shows the crystal plane with a lattice

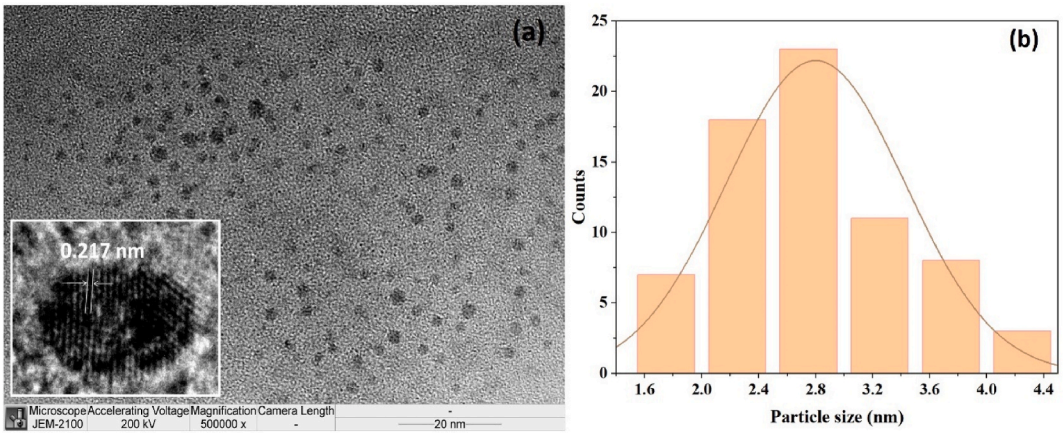

Fig. 2. (a) TEM image of the coffee ground waste-derived CQDs (inset is a zoomed-in image of individual CQD) and (b) particle size distribution of CQDs.

spacing of 0.217 nm, which corresponds to graphitic carbon [34]. The size distribution histogram (Fig. 2b) showed that the particle size of CQDs ranged from 1.6 to 4.4 nm. The average size is 2.80 ± 0.63 nm (obtained from the statistical analysis of 70 particles in the TEM image). These results confirmed the formation of CQDs.

The optical properties of the as-prepared CQD solution were studied through UV–visible absorption and photoluminescence (PL) emission. Fig. 3a shows the adsorption spectrum of the CQD solution in the range of 300–700 nm. The presence of broad adsorption in the visible region represented the photocatalytic activity of CQDs under visible light [24]. The as-prepared CQD solution was light brown under natural daylight and exhibited strong blue-green PL under UV irradiation at 365 nm (Fig. 3b).

From Fig. 3c–d, the PL emission spectra of the as-prepared CQD solution were dependent on excitation wavelengths. This is attributed to their small particle sizes, the electrostatic repulsions between the particles, and the abundance of a hydroxyl group on the surface [35,36]. With the increase of excitation wavelength from 320 to 650 nm (Fig, 3c), the emission peak shifted to the longer wavelengths. The maximum emission peak was observed at 537 nm under the excitation wavelength of 470 nm. This result indicated the down-conversion PL behavior of the CQD solution. The CQD solution also showed the up-conversion PL behavior under the excitation wavelength of 700–900 nm (Fig. 3d). The up-converted emission peak covered the visible light range of 420–700 nm. This result demonstrated that CQDs could expose to near-infrared light and then emit light with shorter wavelengths. The multi-photon absorption process can explain the up-conversion PL behavior, which leads to anti-stokes emission [37].

3.2. Properties of TiO_2 photocatalysts

XRD was used to analyze the crystalline structure and phase of the TiO_2 photocatalysts. XRD patterns of the sol-gel-derived TiO_2 powder are presented in Fig. 4. All samples showed the diffraction peak of anatase. No characteristic peak of CQDs was observed in the diffraction patterns, which is consistent with the previous studies [23,38,39]. This is due to the relatively low diffraction intensity of the CQDs as compared to TiO_2. The crystallite sizes of the TiO_2 powder obtained by sol-gel were calculated by the Scherrer equation [40] using the characteristic peak of anatase TiO_2 ($2\theta = 25.2^\circ$). They are 10.71, 9.75, 8.94 and 8.57 nm for reference TiO_2,

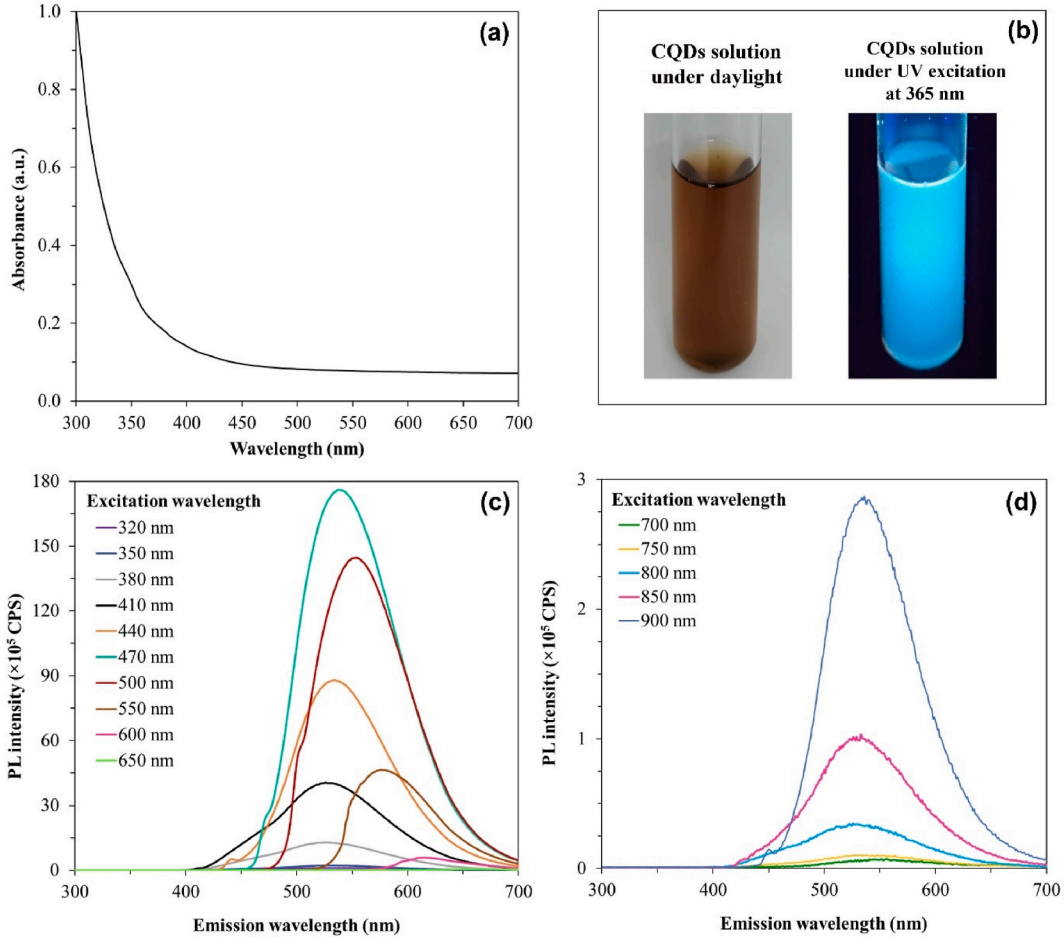

Fig. 3. Optical properties of the coffee ground waste-derived CQD solutions: (a) UV–visible absorption spectrum, (b) photographs of the CQD solution, (c) PL emission spectra, and (d) up-conversion PL emission spectra.

3CQDs/TiO_2, 5CQDs/TiO_2 and 9CQDs/TiO_2, respectively. This is implied that the crystallite size of the sol-gel-derived TiO_2 powder is decreased with increasing CQD solution content. In addition, the XRD pattern of the commercial TiO_2 powder (titania source for coating on FGC in the first step) is also shown in Fig. S1. The samples before and after calcined (500 °C for 1 h) contain pure anatase phase with crystallite sizes of 27.18, and 27.88 nm, respectively. The crystalline phase is still anatase and the crystallite size is not much change because anatase transforms to rutile at the calcination temperature of ~600 °C. Rutile phase has a large crystallite size and high electron-hole recombination rate as compared to anatase [41].

The morphologies of the reference TiO_2 powder (Fig. 5a) and the 5CQDs/TiO_2 powder (Fig. 5b) were characterized by TEM. The lattice spacing of 0.349–0.352 nm corresponded to the (101) crystal plane of anatase TiO_2. The lattice spacing of 0.212–0.218 nm corresponded to the (002) crystal plane of graphitic carbon, indicating the presence of CQDs [36]. This result confirms the hetero-structure of 5CQD/TiO_2, which involves the presence of CQDs on the surface of TiO_2.

The surface functional groups of sol-gel-derived TiO_2 powder were analyzed by FTIR spectroscopy. From Fig. 6a, the absorption band at 3450 and 1632 cm^{-1} indicated the presence of hydroxyl group (-OH) on the surface of sol-gel-derived TiO_2, which helps to promote the photocatalytic activity by increasing the electron transportability [42,43]. For the broad absorption bands in the 400-900 cm^{-1} range, the band is attributed to Ti–O–Ti in the case of the reference TiO_2 (without CQDs) [44]. For the CQDs/TiO_2 samples, the bands show a slight blue shift in wavenumber compared to that of the reference TiO_2. This is attributed to the presence of Ti–O–C in combination with Ti–O–Ti vibrations [45–47].

From Fig. 6b, the peaks of the C–H (1407 cm^{-1}) and COO^- (1387 cm^{-1}) appeared in all samples [34,48], which related to the residue of TiO_2 precursor (titanium butoxide and acetylacetone) from the sol-gel process [49]. Compared to the reference TiO_2, the CQDs/TiO_2 samples showed some new functional groups, including C=O of carbonyl groups (1760 cm^{-1}) and C=C (1562, 1532 and 1448 cm^{-1}) [42,48,50,51]. This observation is due to the surface functional groups of CQDs that can interact with TiO_2. The blue shift of the broad absorption bands in the range of 400–900 cm^{-1} indicates the interaction between TiO_2 and CQDs with the formation of Ti–O–C [45–47].

Photoluminescence measurement is well known technique to investigate the behavior of the photo-excited electrons and holes. The previous works well reported that the PL spectra are caused by the electron-hole recombination process [38,52]. PL spectra of the reference TiO_2 powder and the CQDs/TiO_2 powder at the excitation wavelength of 300 nm are presented in Fig. 7. A lower PL intensity indicates a hindrance to the recombination of the photo-excited electrons and holes in the photocatalyst, which is beneficial to the photocatalytic activity. All samples exhibited similar shapes with different intensities. A broad PL emission in each sample was observed at around 390–470 nm. The PL intensity of all CQDs/TiO_2 samples was lower than that of the reference TiO_2 powder. For CQDs/TiO_2 samples, the PL intensity was on the order of 3CQDs/TiO_2 > 9CQDs/TiO_2 > 5CQDs/TiO_2. This result indicates that the composite of TiO_2 with appropriate amount of CQDs helps to suppress the recombination of the photo-excited electrons and holes in the photocatalyst. However, further increasing the amount of CQDs increase the electron-hole recombination because the excessive CQDs loading reduced the surface active sites of TiO_2 thus increase the probability of collision between the photo-excited electrons and holes [45].

3.3. Properties of TiO_2-coated FGCs

FESEM analysis was used to study the morphologies of TiO_2-coated FGCs. Fig. 8a–d shows the FESEM images of reference TiO_2-coated FGC and CQDs/TiO_2-coated FGC. The FESEM images show that TiO_2 can be coated on flexible FGC using two-step coating procedures without an additional binding agent, which is consistent with the previous report [53]. Fig. 8e shows the schematic illustration of TiO_2-coated FGC. The sol-gel TiO_2 helps to attach the commercial TiO_2 powder to the FGC surface. Meanwhile, the

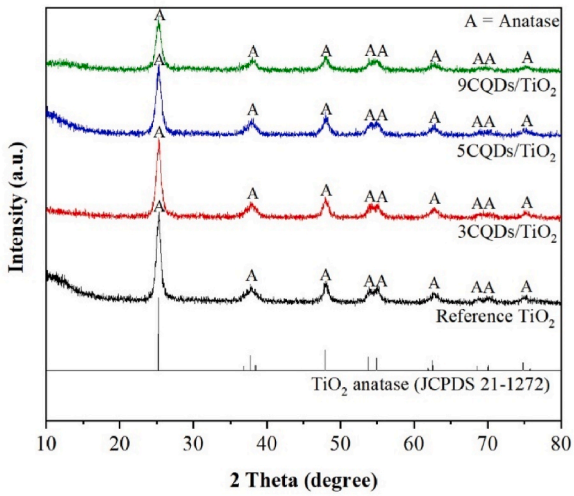

Fig. 4. XRD patterns of the sol-gel derived TiO_2 powder.

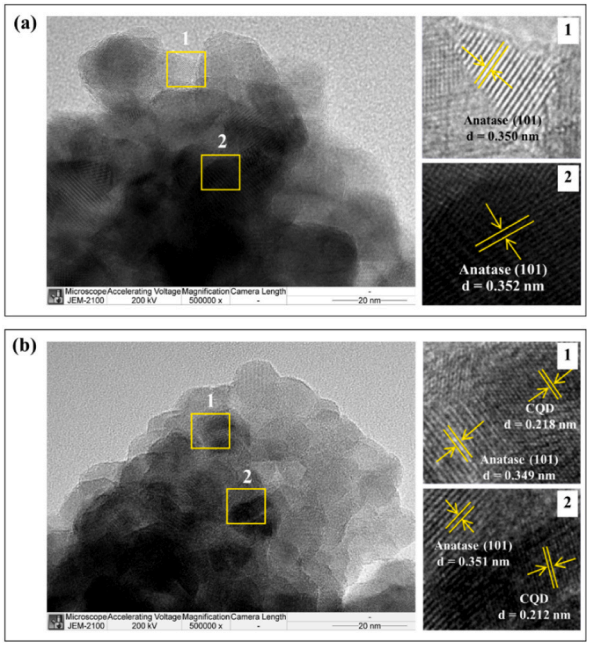

Fig. 5. TEM images of the sol-gel derived TiO_2 powder: (a) reference TiO_2 powder and (b) 5CQDs/TiO_2 powder.

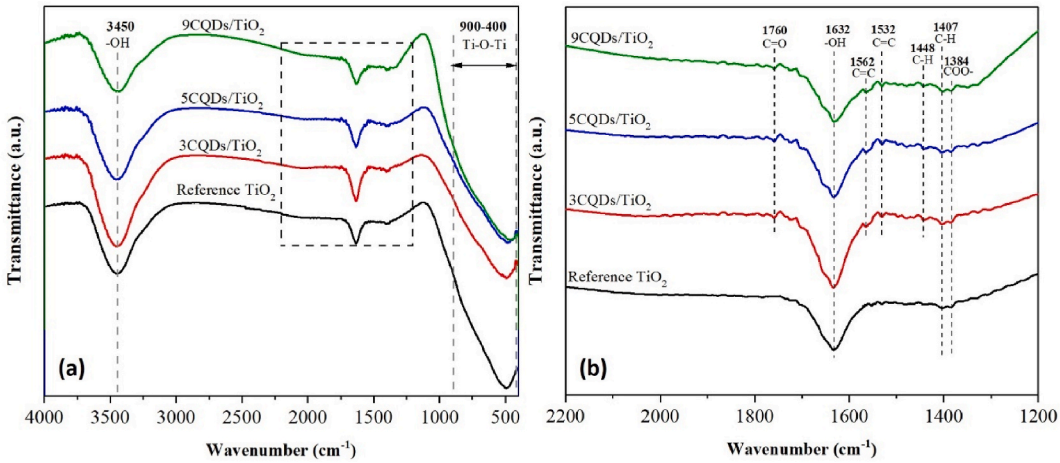

Fig. 6. FTIR spectra of the sol-gel derived TiO_2 powder in the wavenumber range of (a) 4000-480 cm^{-1} and (b) 2200-1200 cm^{-1}.

commercial TiO_2 powder provides the surface roughness of TiO_2 film, which helps to enhance the photocatalytic activity [54].

UV–Visible absorption spectra of the FGC coated with reference TiO_2 and CQDs/TiO_2 are presented in Fig. 9. The FGC coated with reference TiO_2 showed strong absorption in the UV region, and an absorption edge was observed at ~410 nm. The previous studies regarding anatase TiO_2-coated FGC also found an absorption edge in the range of 410–420 nm [55,56]. In the visible region, the absorbances of all FGCs coated with CQDs/TiO_2 were slightly higher than the FGC coated with reference TiO_2. For the bandgap of the samples, only crystalline anatase was identified by XRD in the previous section. Anatase TiO_2 has only an indirect bandgap, which can be estimated by the Kubelka-Munk equation coupled with the Tauc plot methodology (inset of Fig. 9) [33]. The indirect bandgaps were estimated to be 3.08, 3.04, 2.96, and 2.99 eV for the FGC coated with reference TiO_2, 3CQDs/TiO_2, 5CQDs/TiO_2, and 9CQDs/TiO_2, respectively. As compared to the FGC coated with reference TiO_2, the FGCs coated with CQDs/TiO_2 showed a small bandgap narrowing. In addition, the indirect bandgap of reference TiO_2 power was also estimated to be 3.2 eV (Fig. S2), which is slightly higher than that of the reference TiO_2-coated FGC. The value of 3.2 eV is consistent with the theoretical bandgap of anatase TiO_2 [57]. These results demonstrate that the visible light absorption of TiO_2-coated FGC could improve due to the interaction of both FGC and CQDs with TiO_2, which is expected to enhance the photocatalytic activity under visible light.

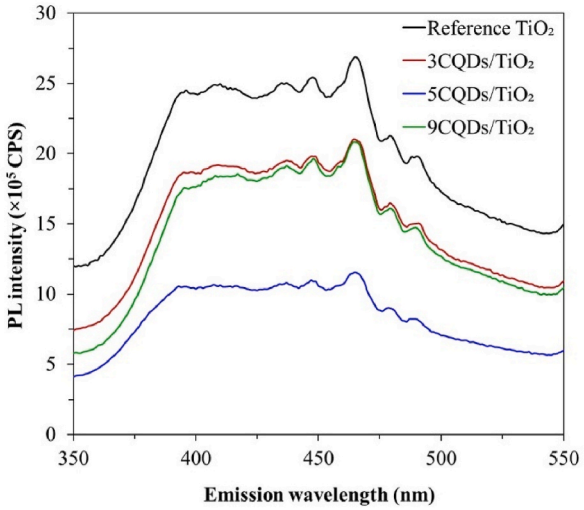

Fig. 7. PL emission spectra of the sol-gel derived TiO_2 powder.

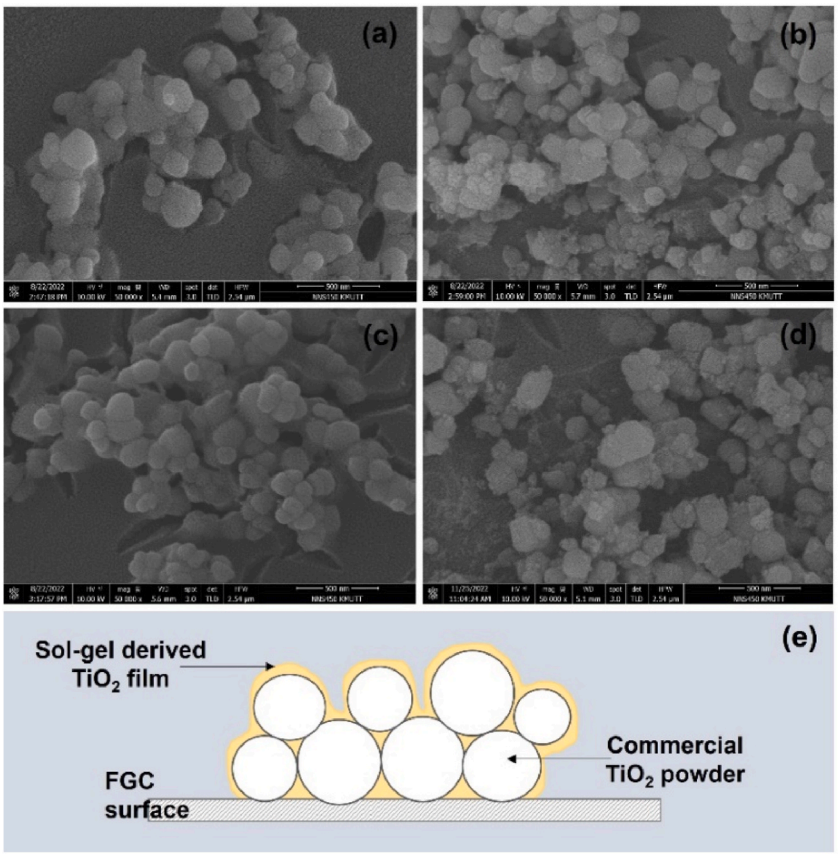

Fig. 8. FESEM images of the FGC coated with (a) reference TiO_2, (b) 3CQDS/TiO_2, (c) 5CQDS/TiO_2, and (d) 9CQDS/TiO_2, and (e) schematic illustration of the TiO_2-coated FGC.

3.4. Photocatalytic removal of pharmaceuticals from water

In the experiments, the initial concentrations of CAF, CBZ, and IBP were individually set based on real values found in their manufacturing wastewater, as reported in the literature [8–10]. Each experiment was conducted in duplicate. The solution

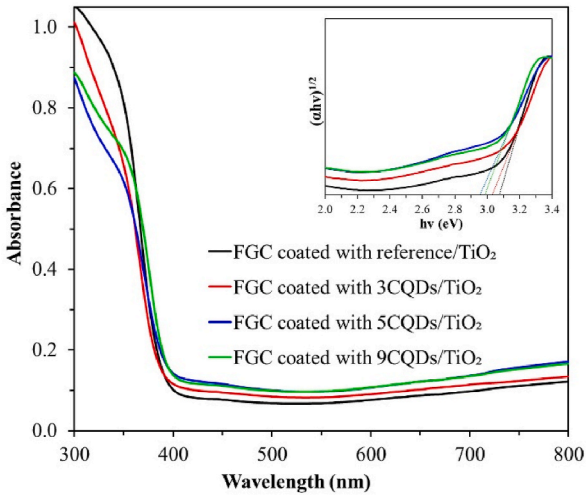

Fig. 9. UV–visible absorption spectra of the TiO_2-coated FGCs with an inset showing the Tauc plots for indirect bandgaps.

evaporation during the experiment was negligible (≤1.2%) because the wastewater temperature was controlled at around 28.5 ± 1.5 °C using a water-cooling system throughout the experiments.

3.4.1. Optimization of CQD contents for CQDs/TiO_2-coated FGC

To optimize CQD content in the CQDs/TiO_2-coated FGC, the photocatalytic experiments were conducted in a simple batch reactor using CAF (3.6 mg/L) as a target pollutant. Before irradiation, the photocatalyst-coated FGC (10 cm × 10 cm) was soaked in CAF solution (60 mL) under horizontal shaking for 3 h to provide an adsorption-desorption desorption equilibrium. Fig. 10a presents the removal of CAF through adsorption in the dark for 3 h and photocatalytic degradation under visible light irradiation for 6 h. The adsorption of CAF on the TiO_2-coated FGCs exhibited efficiencies of 1–3%. Photocatalytic degradation of CAF under visible light irradiation showed that all CQDs/TiO_2-coated FGCs exhibited much higher removal efficiency compared with the TiO_2-coated reference FGCs (without CQDs). Fig. S3 shows that the removal of CAF from water in the presence of a pure CQD solution did not exhibit photocatalytic activity, indicating that the CQD solution cannot act individually as a photocatalyst under visible light irradiation. The results suggest that the interaction between TiO_2 and CQDs significantly enhances the photocatalytic activity, which is consistent with previous reports [19,24].

From Fig. 10b, the most efficient photocatalyst was 5CQDs/TiO_2-coated FGC, with an overall removal efficiency of 72.66%. Therefore, the 5CQDs/TiO_2-coated FGC were selected for further studies in the recirculating reactor. However, the removal efficiency cannot be directly compared to previous reports because of the different preparation methods for photocatalysts and the different operational conditions for the photocatalytic processes.

According to the mechanism reported in the literature, the visible-light-driven photocatalytic activity of the CQDs/TiO_2 composite is enhanced due to the up-conversion PL of CQDs and the efficient electron-hole pair separation [37,58–60]. From the up-conversion

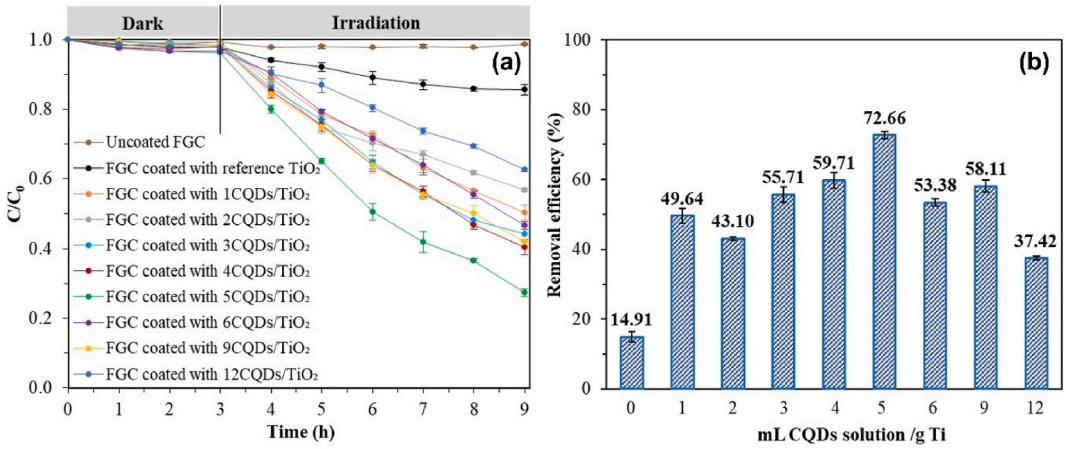

Fig. 10. Visible light-driven photocatalytic degradation of CAF in the simple batch reactor for 6 h using CQDs/TiO_2-coated FGC with different CQD contents: (a) degradation ratio respecting the time and (b) removal efficiency respecting the ratio of mL CQD solution to g Ti.

PL spectra of the CQD solution (Fig. 3d), the emission wavelengths covered 420–700 nm, which cannot provide enough energy to excite the TiO_2 without CQDs. From Fig. 9, the FGCs coated with CQDs/TiO_2 have better light absorption and lower bandgaps than the FGCs coated with reference TiO_2. Therefore, the lower PL intensity of the PL spectra of CQDs/TiO_2 (Fig. 7) is due to an obstruction of the recombination of the photo-excited electrons and holes in the photocatalyst [38,61]. The electron-hole recombination rate was in the order of reference TiO_2 > 3CQDs/TiO_2 > 9CQDs/TiO_2 > 5CQDs/TiO_2.

For photocatalytic degradation of CAF using the CQDs/TiO_2-coated FGCs under visible light irradiation, a trend of removal efficiency (Fig. 10b) is consistent with the electron-hole recombination result. The photocatalyst with lower electron-hole recombination can provide higher photocatalytic activity. From Fig. 10a and b, 5CQDs/TiO_2-coated FGC showed the highest removal efficiency (72.66%) because the electron-hole recombination in 5CQDs/TiO_2 was lower than other photocatalysts. Therefore, a plausible mechanism is presented in Fig. 11. CQDs play the role of photosensitizers, which can inject the excited electron into TiO_2. When the CQDs/TiO_2 composite is irradiated by visible light, the ground state electrons of CQDs can be excited to their LUMO level and leave the holes at the ground state. The excited electrons can transfer to the conduction band (CB) of TiO_2 and then react with the adsorbed oxygen molecules (O_2) to produce the superoxide radicals ($^{\bullet}O_2^-$). Meanwhile, the holes can react with the adsorbed water molecules (H_2O) or the hydroxide ions (OH^-) to produce the hydroxyl radicals ($^{\bullet}OH$). The superoxide radicals ($^{\bullet}O_2^-$) and hydroxyl radicals ($^{\bullet}OH$) can eventually degrade the organic pollutants (such as pharmaceutical pollutants) [37,58–60,62].

3.4.2. Photocatalytic degradation of pharmaceuticals in the recirculating reactor

3.4.2.1. Influence of irradiation time. The effect of irradiation time on the photocatalytic degradation of CAF, CBZ, and IBP from water was studied individually using the initial concentrations of each pharmaceutical as found in their production effluents (CAF = 3.6 mg/L, CBZ = 0.6 mg/L, and IBP = 1.7 mg/L). The experiments were conducted at the inherent solution pH of 7.2 ± 0.1 for CAF, 7.3 ± 0.1 for CBZ, and 6.1 ± 0.1 for CBZ. It is beneficial to reduce operating costs if the wastewater can be treated without any pH adjustment, especially in large-scale applications.

From Fig. 12a, the experiments include adsorption in the dark for 3 h followed by photocatalysis under visible light irradiation for 9 h. The overall removal efficiencies of CAF, CBZ, and IBP were 82%, 88%, and 84%, corresponding to the residual concentrations of 0.63 mg/L, 0.08 mg/L, and 0.27 mg/L, respectively. In comparison with the toxicity values reported in the literature, these residual concentrations are significantly below their lowest observed effect concentrations (LOEC) for fish (0.91 mg/L CAF) [6], water flea (0.1 mg/L CBZ) [11], and diatoms (1 mg/L IBP) [12].

From Fig. 12b, the mineralizations of CAF, CBZ, and IBP were studied through the measurement of total organic carbon (TOC), which are 59%, 43%, and 48%, respectively. The results demonstrated that the 5CQDs/TiO_2-coated FGC has the potential for degradation and mineralization of pharmaceutical pollutants from water. The mineralization rates were found to be slower than the pharmaceutical degradation rates, agreeing with the previous reports [63,64]. This result indicates the presence of some intermediate species. However, the toxicity of the intermediates from the photocatalytic degradation of CBZ and IBP was lower than that of the parent compounds. Based on fish, daphnia, and green algae, the intermediates from the photocatalytic degradation of CAF showed the same toxicity as CAF [65].

3.4.2.2. Influence of initial pharmaceutical concentration. Kinetic studies on the photocatalytic degradation of pharmaceutical pollutants are essential to understand the condition for the future design of the large-scale application. The influences of initial concentration of CAF (3–5 mg/L), CBZ (0.6–1.2 mg/L), and IBP (1.4–2.4 mg/L) were investigated for kinetic studies using the method of initial rates (Equations (1) and (2)) coupled with Langmuir-Hinshelwood model (Equations (3) and (4)).

$$r_{e,0} = \frac{-dc}{dt} = -k_{app} C_{e,0} \tag{1}$$

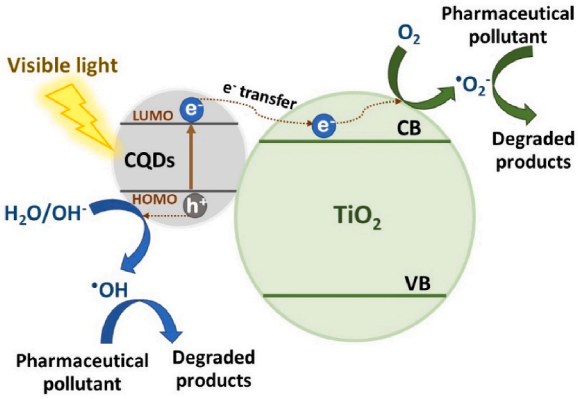

Fig. 11. Proposed photocatalytic mechanism of CQDs/TiO_2 composite.

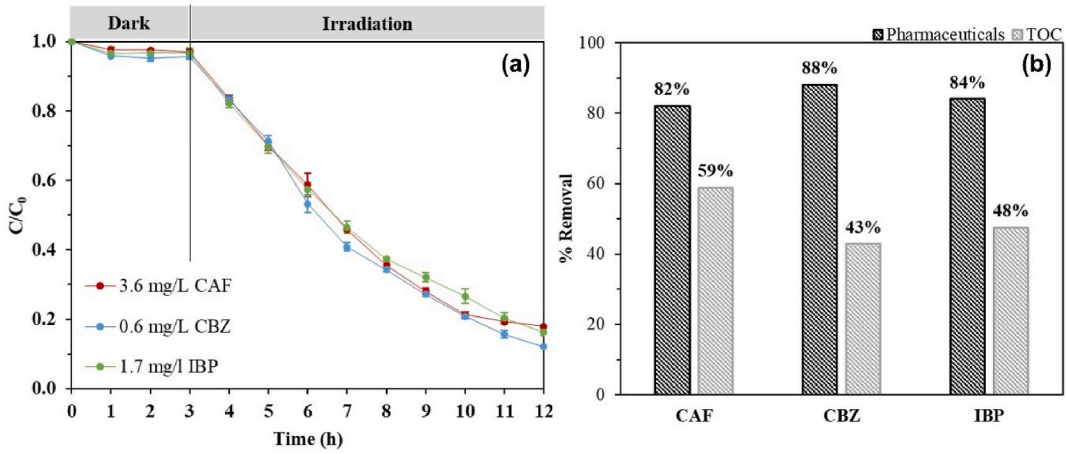

Fig. 12. Photocatalytic degradation of pharmaceuticals in the recirculating reactor: (a) degradation ratio respecting the time and (b) pharmaceutical removal efficiencies and TOC removal efficiencies after 9 h of visible light irradiation.

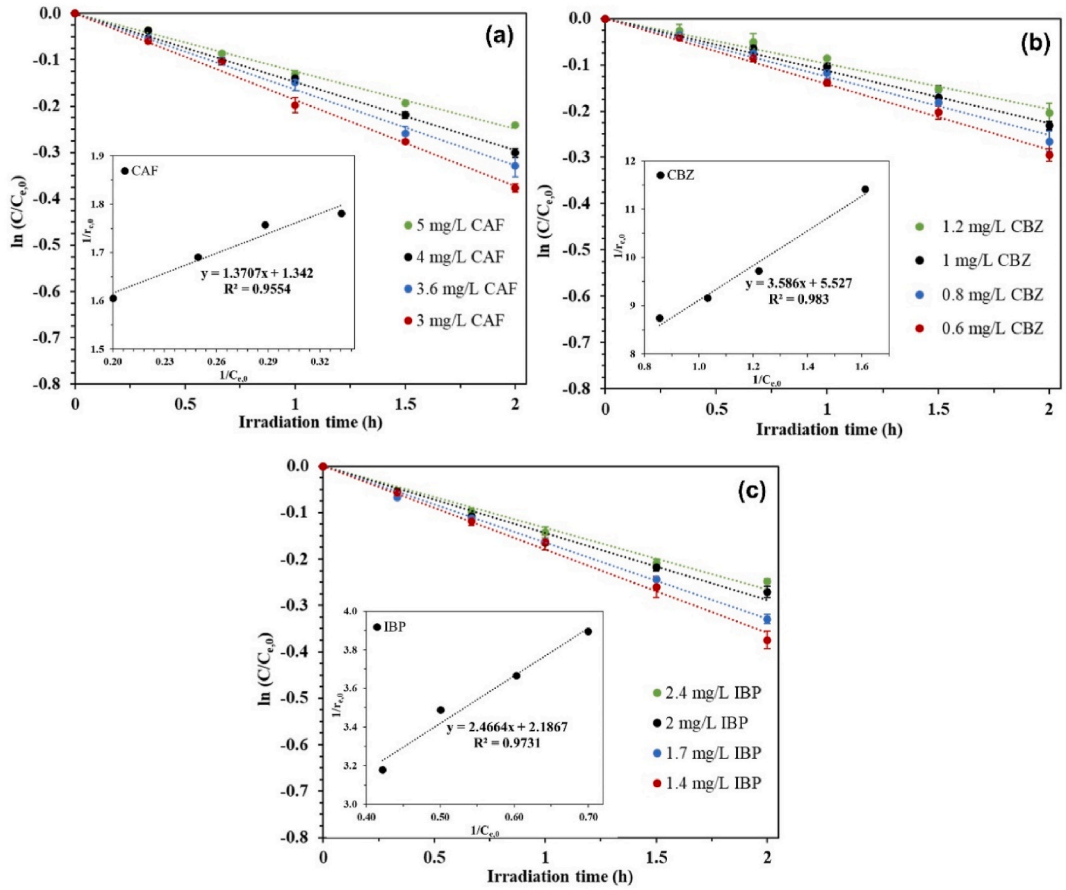

Fig. 13. Pseudo-first-order kinetic plots for the photocatalytic degradation of (a) CAF, (b) CBZ, and (c) IBP using 5CQDs/TiO_2-coated FGC under visible light irradiation. The insets show the linearization of the Langmuir-Hinshelwood model.

$$\ln (C/C_{e,0}) = -k_{app}t \quad (2)$$

$$r_{e,0} = \frac{kKC_{e,0}}{1 + KC_{e,0}} \quad (3)$$

$$\frac{1}{r_{e,0}} = \frac{1}{k} + \frac{1}{kKC_{e,0}} \quad (4)$$

where $r_{e,0}$ is the initial photocatalytic reaction rate (mg/L·h), k_{app} is the apparent rate constant (h^{-1}), C is the initial concentration of pharmaceutical (mg/L), $C_{e,0}$ is the equilibrium concentration after adsorption in the dark (mg/L), t is irradiation time (h), k is the reaction rate constant (mg/L·h), and K is the dynamic Langmuir adsorption constant (L/mg) [66,67].

All photocatalytic experiments were run for 6 h under visible light irradiation, as shown in Figs. S4a–S4c. The order of reaction was determined by the method of initial rates using the experimental data during the first 2 h under visible light irradiation. Fig. 13a–c shows the kinetic fitting results for four different initial concentrations of each pharmaceutical. The photocatalytic reaction was well-described by the pseudo-first-order kinetic model in accordance with those reported in previous studies [66,68,69]. The slope of the line represents the apparent rate constants (k_{app}). The initial reaction rates ($r_{e,0}$) were calculated from Equation (1) and sequentially fitted by the linearity equation of the Langmuir-Hinshelwood model (Equation (4)). The values of k and K were determined from the plots of $1/r_{e0}$ against $1/C_{e,0}$ (Insets of Fig. 13a–c). The obtained kinetic parameters are summarized in Table 1.

In the studied concentration ranges, the values of k_{app} decreased with increasing the initial concentrations of CAF, CBZ, and IBP. This could be explained that the increase in pharmaceutical concentration leads to (i) low photon penetration into the solutions and (ii) a large number of pharmaceutical molecules adsorbed on the photocatalyst surface, reducing the surface-adsorbed hydroxide ions and oxygen molecules, resulting in the decrease of free radical formation [70]. The photocatalytic degradation of CAF, CBZ, and IBP could be described by substituting the values of k and K in the Langmuir-Hinshelwood model (Equation (3)). The relationship between the equilibrium concentration of pharmaceuticals and the initial photocatalytic reaction rate could be written as Equations (5)–(7).

$$\text{For CAF}: r_{e,0} = \frac{0.7296C_{e,0}}{1 + 0.9791C_{e,0}} \quad (5)$$

$$\text{For CBZ}: r_{e,0} = \frac{0.2788C_{e,0}}{1 + 1.541C_{e,0}} \quad (6)$$

$$\text{For IBP}: r_{e,0} = \frac{0.4054C_{e,0}}{1 + 0.8866C_{e,0}} \quad (7)$$

3.4.2.3. Reusable and flexible performance of FGC coated with CQDs/TiO_2. In order to investigate the reusable and flexible performance of 5CQDs/TiO_2-coated FGC, the photocatalytic degradation of CAF (3.6 mg/L) was repeated for five cycles under visible light irradiation. After each cycle, the 5CQDs/TiO_2-coated FGC were thoroughly washed with ultrapure water, exposed to the sun for one day, and sequentially rolled and kept in a cylindrical container for 12 h before reuse. The photocatalytic reaction was run for 7 h in each cycle to achieve the lowest observed effect concentration (LOEC) for fish (0.91 mg/L) [6]. From Fig. 14, the removal efficiencies were relatively stable (77–79%) after five runs. The result demonstrates a good reusable and flexible performance of 5CQDs/TiO_2-coated FGC. Therefore, it can be folded into many shapes, which provides the opportunity to use in various types of photocatalytic reactors in practical applications.

3.4.2.4. CAF removal in actual wastewater. The actual wastewater was collected from the coffee pot cleaning process. The photocatalytic degradation of CAF in actual wastewater was conducted to evaluate the applicability of 5CQDs/TiO_2-coated FGC in the recirculating reactor (Fig. 15). The initial concentration of CAF in actual wastewater was 3.92 mg/L, and the initial color was 388 ADMI. The experiments were run through adsorption in the dark for 3 h followed by visible light irradiation for 12 h. The treated water showed a remaining CAF concentration of 0.79 mg/L (removal efficiency ~80%), which is below the LOEC for fish (0.91 mg/L) [6]. The remaining color was 54 ADMI, which is significantly lower than the industrial effluent standard (300 ADMI) [71].

4. Conclusion

CQD solutions have been successfully prepared by hydrothermal method using the coffee ground waste as a raw waste material. The visible light-sensitive photocatalysts were synthesized by composite TiO_2 with the coffee ground-derived CQDs, and then coated on FGCs. The main results can be concluded as follows:

(1) The optimum photocatalyst was 5CQDs/TiO_2-coated FGC (5 mL of CQD solution/g of Ti), which efficiently removed CAF, CBZ, and IBP from water in the recirculating reactor. The residual concentrations of CAF, CBZ, and IBP achieved their reported toxicity levels based on fish, water fleas, and diatoms.
(2) The 5CQDs/TiO_2-coated FGC showed good reusability and flexibility in use, and it could be easily regenerated by exposure to natural sunlight.

Table 1
Kinetic parameters for the photocatalytic degradation of CAF, CBZ, and IBP.

Pollutant	C_0 (mg/L)	k_{app} (h^{-1})	$r_{e,0}$ (mg/L·h)	k (mg/L·h)	K (L/mg)
CAF	3	0.1865	0.5614	0.7452	0.9791
	3.6	0.1640	0.5691		
	4	0.1475	0.5915		
	5	0.1246	0.6230		
CBZ	0.6	0.1413	0.0876	0.1809	1.5413
	0.8	0.1255	0.1029		
	1	0.1126	0.1092		
	1.2	0.0978	0.1144		
IBP	1.4	0.1795	0.2567	0.4573	0.8866
	1.7	0.1643	0.2727		
	2	0.1433	0.2866		
	2.4	0.1327	0.3145		

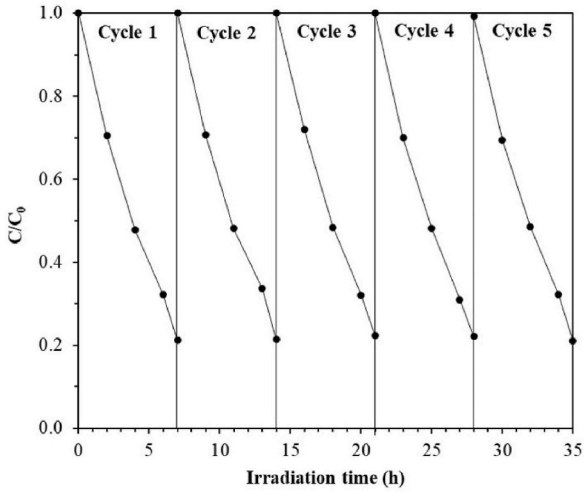

Fig. 14. Photocatalytic degradations of CAF under visible light irradiation for five cycles.

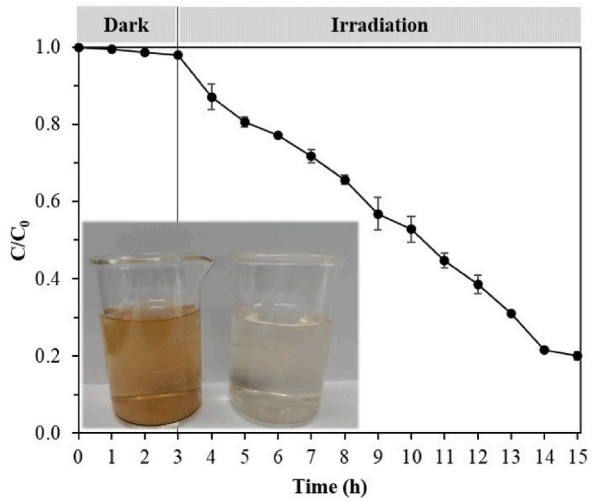

Fig. 15. Removal of CAF from actual wastewater. Inset is a photograph of actual wastewater before (left) and after treatment (right) (adsorption for 3 h followed by visible light irradiation for 12 h).

(3) The treatment of coffee-pot cleaning wastewater (actual wastewater) showed high removal efficiencies of 80% for CAF and 86% for ADMI color, which was not harmful to the environment.

Author contribution statement

Conceived and designed the experiments; Patiya Kemacheevakul, Surawut Chuangchote
Performed the experiments; Rattana Muangmora
Analyzed and interpreted the data; Rattana Muangmora, Patiya Kemacheevakul, Surawut Chuangchote
Contributed reagents, materials, analysis tools; Surawut Chuangchote, Patiya Kemacheevakul
Wrote the paper; Rattana Muangmora, Patiya Kemacheevakul, Surawut Chuangchote.

Data availability statement

Data included in article/supp. material/referenced in article.

Declaration of competing interest

The authors declare that they have no known competing financial interests or personal relationships that could have appeared to influence the work reported in this paper.

Acknowledgment

The author (R. Muangmora) would like to acknowledge the Petchra Pra Jom Klao Ph.D. Research Scholarship from King Mongkut's University of Technology Thonburi. This research project was supported by Thailand Science Research and Innovation. Basic Research Fund: The fiscal year 2022 under project number FRB650048/0164. Technical support from the Department of Environmental Engineering, Department of Tool and Materials Engineering, and Department of Food Engineering, King Mongkut's University of Technology Thonburi, is also gratefully acknowledged.

Abbreviation

CAF	Caffeine
CBZ	Carbamazepine
IBP	Ibuprofen
CQDs	Carbon quantum dots
FGC	Fiberglass Cloth

Appendix A. Supplementary data

Supplementary data to this article can be found online at https://doi.org/10.1016/j.heliyon.2023.e17693.

References

[1] S. Mayson, I. Williams, Applying a circular economy approach to valorize spent coffee grounds, Resour. Conserv. Recycl. 172 (2021) 105659–105671.
[2] M. Bekirogullari, Hydrogen production from sodium borohydride by $ZnCl_2$ treated defatted spent coffee ground catalyst, Int. J. Hydrogen Energy 45 (2020) 9733–9743.
[3] M.J. Kim, S.W. Choi, H. Kim, S. Mun, K.B. Lee, Simple synthesis of spent coffee ground-based microporous carbons using K_2CO_3 as an activation agent and their application to CO_2 capture, Chem. Eng. J. 397 (2020) 125404–125414.
[4] A.S. Fernandes, F.V.C. Mello, S. Thode Filho, R.M. Carpes, J.G. Honório, M.R.C. Marques, I. Felzenszwalb, E.R.A. Ferraz, Impacts of discarded coffee waste on human and environmental health, Ecotoxicol. Environ. Saf. 141 (2017) 30–36.
[5] Q. Sui, X. Cao, S. Lu, W. Zhao, Z. Qiu, G. Yu, Occurrence, sources and fate of pharmaceuticals and personal care products in the groundwater: a review, Emerg. Contam. 1 (2015) 14–24.
[6] M. Li, Q. Mei, D. Han, B. Wei, Z. An, H. Cao, J. Xie, M. He, The roles of $HO^{\bullet}$, $ClO^{\bullet}$ and $BrO^{\bullet}$ radicals in caffeine degradation: a theoretical study, Sci. Total Environ. 768 (2021) 144733–144742.
[7] W.J. Sim, J.W. Lee, E.S. Lee, S.K. Shin, S.R. Hwang, J.E. Oh, Occurrence and distribution of pharmaceuticals in wastewater from households, livestock farms, hospitals and pharmaceutical manufactures, Chemosphere 82 (2011) 179–186.
[8] N.H. Tran, J. Li, J. Hu, S.L. Ong, Occurrence and suitability of pharmaceuticals and personal care products as molecular markers for raw wastewater contamination in surface water and groundwater, Environ. Sci. Pollut. Res. 21 (2014) 4727–4740.
[9] S. Kleywegt, M. Payne, F. Ng, T. Fletcher, Environmental loadings of active pharmaceutical ingredients from manufacturing facilities in Canada, Sci. Total Environ. 646 (2019) 257–264.
[10] M. Ashfaq, K.N. Khan, M.S.U. Rehman, G. Mustafa, M.F. Nazar, Q. Sun, J. Iqbal, S.I. Mulla, C.P. Yu, Ecological risk assessment of pharmaceuticals in the receiving environment of pharmaceutical wastewater in Pakistan, Ecotoxicol, Environ. Saf. 136 (2017) 31–39.
[11] F.I. Hai, S. Yang, M.B. Asif, V. Sencadas, S. Shawkat, M. Sanderson-Smith, J. Gorman, Z.Q. Xu, K. Yamamoto, Carbamazepine as a possible anthropogenic marker in water: occurrences, toxicological effects, regulations and removal by wastewater treatment technologies, Water 10 (2018) 107–138.

[12] T. Ding, M. Yang, J. Zhang, B. Yang, K. Lin, J. Li, J. Gan, Toxicity, degradation, and metabolic fate of ibuprofen on freshwater diatom Navicula sp, J. Hazard Mater. 330 (2017) 127–134.
[13] M. Patel, R. Kumar, K. Kishor, T. Mlsna, J.C.U. Pittman, D. Mohan, Pharmaceuticals of emerging concern in aquatic systems: chemistry, occurrence, effects, and removal methods, Chem. Rev. 119 (2019) 3510–3673.
[14] A. Olasupo, F.B.M. Suah, Recent advances in the removal of pharmaceuticals and endocrine-disrupting compounds in the aquatic system: a case of polymer inclusion membranes, J. Hazard Mater. 406 (2021), 124317.
[15] A. Fattahi, M.J. Arlos, L.M. Bragg, S. Kowalczyk, R. Liang, O.M. Schneider, N. Zhou, M.R. Servos, Photodecomposition of pharmaceuticals and personal care products using P25 modified with Ag nanoparticles in the presence of natural organic matter, Sci. Total Environ. 752 (2021) 142000–142010.
[16] A.A. Isari, M. Mehregan, S. Mehregan, F. Hayati, R.R. Kalantary, B. Kakavandi, Sono-photocatalytic degradation of tetracycline and pharmaceutical wastewater using WO_3/CNT heterojunction nanocomposite under US and visible light irradiations: a novel hybrid system, J. Hazard Mater. 390 (2020) 122050–122063.
[17] Q. Zhang, R. Du, C. Tan, P. Chen, G. Yu, S. Deng, Efficient degradation of typical pharmaceuticals in water using a novel TiO_2/ONLH nano-photocatalyst under natural sunlight, J. Hazard Mater. 403 (2021) 123582–123591.
[18] Z. Shayegan, C.S. Lee, F. Haghighat, TiO_2 photocatalyst for removal of volatile organic compounds in gas phase–A review, Chem. Eng. J. 334 (2018) 2408–2439.
[19] N. Xu, H. Huang, H. Ouyang, H. Wang, Preparation of the heterojunction catalyst N-doping carbon quantum dots/P25 and its visible light photocatalytic activity, Sci. Rep. 9 (2019) 1–10.
[20] V. Silva, I. Invėncio, C.P. Silva, M. Otero, D.L. Lima, Photodegradation of oxolinic acid in aquaculture effluents under solar irradiation: is it possible to enhance efficiency by the use of TiO_2/carbon quantum dots composites? Chemosphere 308 (2022) 136522–136532.
[21] C. Kang, Y. Huang, H. Yang, X.F. Yan, Z.P. Chen, A review of carbon dots produced from biomass wastes, Nanomaterials 10 (2020) 2316–2339.
[22] P. Chen, F. Wang, Z.F. Chen, Q. Zhang, Y. Su, L. Shen, K. Yao, Y. Liu, Z. Cai, W. Lv, Study on the photocatalytic mechanism and detoxicity of gemfibrozil by a sunlight-driven TiO_2/carbon dots photocatalyst: the significant roles of reactive oxygen species, Appl. Catal. B Environ. 204 (2017) 250–259.
[23] W. Wang, Y. Ni, Z. Xu, One-step uniformly hybrid carbon quantum dots with high-reactive TiO_2 for photocatalytic application, J. Alloys Compd. 622 (2015) 303–308.
[24] R. Miao, Z. Luo, W. Zhong, S.Y. Chen, T. Jiang, B. Dutta, Y. Nasr, Y. Zhang, S.L. Suib, Mesoporous TiO_2 modified with carbon quantum dots as a high-performance visible light photocatalyst, Appl. Catal. B Environ. 189 (2016) 26–38.
[25] L. Wang, W. Li, B. Wu, Z. Li, S. Wang, Y. Liu, D. Pan, M. Wu, Facile synthesis of fluorescent graphene quantum dots from coffee grounds for bioimaging and sensing, Chem. Eng. J. 300 (2016) 75–82.
[26] D.M. Crista, A. El Mragui, M. Algarra, J.C. Esteves da Silva, R. Luque, L. Pinto da Silva, Turning spent coffee grounds into sustainable precursors for the fabrication of carbon dots, Nanomaterials 10 (2020) 1209–1225.
[27] A.I. Costa, P.D. Barata, B. Moraes, J.V. Prata, Carbon dots from coffee grounds: synthesis, characterization, and detection of noxious nitroanilines, Chemosensors 10 (2022) 113–129.
[28] K. Bankoti, A.P. Rameshbabu, S. Datta, B. Das, A. Mitra, S. Dhara, Onion derived carbon nanodots for live cell imaging and accelerated skin wound healing, J. Mater. Chem. B 5 (2017) 6579–6592.
[29] Y.Y. Yao, G. Gedda, W.M. Girma, C.L. Yen, Y.C. Ling, J.Y. Chang, Magnetofluorescent carbon dots derived from crab shell for targeted dual-modality bioimaging and drug delivery, ACS Appl. Mater. Interfaces 9 (2017) 13887–13899.
[30] D.B. Gunjal, V.M. Naik, R.D. Waghmare, C.S. Patil, R.V. Shejwal, A.H. Gore, G.B. Kolekar, Sustainable carbon nanodots synthesised from kitchen derived waste tea residue for highly selective fluorimetric recognition of free chlorine in acidic water: a waste utilization approach, J. Taiwan Inst. Chem. Eng. 95 (2019) 147–154.
[31] Z. Liu, P. Fang, S. Wang, Y. Gao, F. Chen, F. Zheng, Y. Liu, Y. Dai, Photocatalytic degradation of gaseous benzene with CdS-sensitized TiO_2 film coated on fiberglass cloth, J. Mol. Catal. Chem. 363 (2012) 159–165.
[32] T.D. Pham, B.K. Lee, Feasibility of silver doped TiO_2/glass fiber photocatalyst under visible irradiation as an indoor air germicide, Int. J. Environ. Res. Publ. Health 11 (2014) 3271–3288.
[33] K. Roongraung, S. Chuangchote, N. Laosiripojana, Enhancement of photocatalytic oxidation of glucose to value-added chemicals on TiO_2 photocatalysts by a zeolite (Type y) support and metal loading, Catalysts 10 (2020) 423–438.
[34] M. He, J. Zhang, H. Wang, Y. Kong, Y. Xiao, W. Xu, Material and optical properties of fluorescent carbon quantum dots fabricated from lemon juice via hydrothermal reaction, Nanoscale Res. Lett. 13 (2018) 1–7.
[35] A.M. Alam, B.Y. Park, Z.K. Ghouri, M. Park, H.Y. Kim, Synthesis of carbon quantum dots from cabbage with down-and up-conversion photoluminescence properties: excellent imaging agent for biomedical applications, Green Chem. 17 (2015) 3791–3797.
[36] Y. Deng, M. Chen, G. Chen, W. Zou, Y. Zhao, H. Zhang, Q. Zhao, Visible-ultraviolet upconversion carbon quantum dots for enhancement of the photocatalytic activity of titanium dioxide, ACS Omega 6 (2021) 4247–4254.
[37] J. Ke, X. Li, Q. Zhao, B. Liu, S. Liu, S. Wang, Upconversion carbon quantum dots as visible light responsive component for efficient enhancement of photocatalytic performance, J. Colloid Interface Sci. 496 (2017) 425–433.
[38] S. Sharma, A. Umar, S.K. Mehta, A.O. Ibhadon, S.K. Kansal, Solar light driven photocatalytic degradation of levofloxacin using TiO_2/carbon-dot nanocomposites, New J. Chem. 42 (2018) 7445–7456.
[39] D. Choi, S. Ham, D.J. Jang, Visible-light photocatalytic reduction of Cr (VI) via carbon quantum dots-decorated TiO_2 nanocomposites, J. Environ. Chem. Eng. 6 (2018) 1–8.
[40] K. Sirirerkratana, P. Kemacheevakul, S. Chuangchote, Color removal from wastewater by photocatalytic process using titanium dioxide-coated glass, ceramic tile, and stainless-steel sheets, J. Clean. Prod. 215 (2019) 123–130.
[41] N. Yuangpho, S.T.T. Le, T. Treerujiraphapong, W. Khanitchaidecha, A. Nakaruk, Enhanced photocatalytic performance of TiO_2 particles via effect of anatase-rutile ratio, Physica E Low Dimens. Syst. Nanostruct. 67 (2015) 18–22.
[42] Y. Fu, G. Gao, J. Zhi, Electrochemical synthesis of multicolor fluorescent N-doped graphene quantum dots as a ferric ion sensor and their application in bioimaging, J. Mater. Chem. B 7 (2019) 1494–1502.
[43] A.K. John, S. Palaty, S.S. Sharma, Greener approach towards the synthesis of titanium dioxide nanostructures with exposed {001} facets for enhanced visible light photodegradation of organic pollutants, J. Mater. Sci. Mater. Electron. 31 (2020) 20868–20882.
[44] G. Gohari, A. Mohammadi, A. Akbari, S. Panahirad, M.R. Dadpour, V. Fotopoulos, S. Kimura, Titanium dioxide nanoparticles (TiO_2 NPs) promote growth and ameliorate salinity stress effects on essential oil profile and biochemical attributes of Dracocephalum moldavica, Sci. Rep. 10 (2020) 1–14.
[45] H. Zhang, X. Wang, N. Li, J. Xia, Q. Meng, J. Ding, J. Lu, Synthesis and characterization of TiO_2/graphene oxide nanocomposites for photoreduction of heavy metal ions in reverse osmosis concentrate, RSC Adv. 8 (2018) 34241–34251.
[46] M. Kocijan, L. Ćurković, D. Ljubas, K. Mužina, I. Bačić, T. Radošević, M. Podlogar, I. Bdikin, G. Otero-Irurueta, M.J. Hortigüela, Graphene-based TiO_2 nanocomposite for photocatalytic degradation of dyes in aqueous solution under solar-like radiation, Appl. Sci. 11 (2021) 3966–3980.
[47] A. Nasir, S. Khalid, T. Yasin, A. Mazare, A Review on the progress and future of TiO_2/graphene photocatalysts, Energies 15 (2022) 6248–6281.
[48] B. Thangaraj, S. Chuangchote, N. Wongyao, P.R. Solomon, K. Roongraung, W. Chaiworn, W. Surareungchai, Flexible sodium-ion batteries using electrodes from Samanea saman tree leaf-derived carbon quantum dots decorated with SnO_2 and $NaVO_3$, Clean Energy 5 (2021) 354–374.
[49] P. Khodaparast, Z. Ounaies, Influence of dispersion states on the performance of polymer-based nanocomposites, Smart Mater. Struct. 23 (2014) 104004–104018.
[50] A. Lauria, E. Lizundia, Luminescent carbon dots obtained from polymeric waste, J. Clean. Prod. 262 (2020) 121288–121296.
[51] X. Yan, S. Rahman, M. Rostami, Z.A. Tabasi, F. Khan, A. Alodhayb, Y. Zhang, Carbon quantum dot-incorporated chitosan hydrogel for selective sensing of Hg^{2+} ions: synthesis, characterization, and density functional theory calculation, ACS Omega 6 (2021) 23504–23514.
[52] Y. Sui, L. Wu, S. Zhong, Q. Liu, Carbon quantum dots/TiO_2 nanosheets with dominant (001) facets for enhanced photocatalytic hydrogen evolution, Appl. Surf. Sci. 480 (2019) 810–816.

[53] S. Horikoshi, N. Watanabe, H. Onishi, H. Hidaka, N. Serpone, Photodecomposition of a nonylphenol polyethoxylate surfactant in a cylindrical photoreactor with TiO_2 immobilized fiberglass cloth, Appl. Catal. B Environ. 37 (2002) 117–129.
[54] C.C. Kuo, Y.R. Chen, A new method to characterizing surface roughness of TiO_2 thin films, Opt Laser. Eng. 49 (2011) 410–414.
[55] S. Lin, X. Zhang, Q. Sun, T. Zhou, J. Lu, Fabrication of solar light induced Fe-TiO_2 immobilized on glass-fiber and application for phenol photocatalytic degradation, Mater. Res. Bull. 48 (2013) 4570–4575.
[56] S.B. Yang, H.H. Chun, R.J. Tayade, W.K. Jo, Iron-functionalized titanium dioxide on flexible glass fibers for photocatalysis of benzene, toluene, ethylbenzene, and o-xylene (BTEX) under visible-or ultraviolet-light irradiation, J. Air Waste Manag. Assoc. 65 (2015) 365–373.
[57] T. Zhou, S. Chen, L. Li, J. Wang, Y. Zhang, J. Li, J. Bai, L. Xia, Q. Xu, M. Rahim, Carbon quantum dots modified anatase/rutile TiO_2 photoanode with dramatically enhanced photoelectrochemical performance, Appl. Catal. B Environ. 269 (2020) 118776–118785.
[58] Y.Q. Zhang, D.K. Ma, Y.G. Zhang, W. Chen, S.M. Huang, N-doped carbon quantum dots for TiO_2-based photocatalysts and dye-sensitized solar cells, Nano Energy 2 (2013) 545–552.
[59] G.B. Markad, S. Kapoor, S.K. Haram, P. Thakur, Metal free, carbon-TiO_2 based composites for the visible light photocatalysis, Sol. Energy 144 (2017) 127–133.
[60] C. Xie, T. Fan, A. Wang, S.L. Chen, Enhanced visible-light photocatalytic activity of a TiO_2 membrane-assisted with N-doped carbon quantum dots and SiO_2 opal photonic crystal, Ind. Eng. Chem. Res. 58 (2018) 120–127.
[61] X. Jin, R. Che, J. Yang, Y. Liu, X. Chen, Y. Jiang, J. Liang, S. Chen, H. Su, Activated carbon and carbon quantum dots/titanium dioxide composite based on waste rice noodles: simultaneous synthesis and application in water pollution control, Nanomaterials 12 (2022) 472–492.
[62] D. Awfa, M. Ateia, M. Fujii, M.S. Johnson, C. Yoshimura, Photo-degradation of pharmaceuticals and personal care products in water treatment using carbonaceous-TiO_2 composites: a critical review of recent literature, Water Res. 142 (2018) 26–45.
[63] A. Carabin, P. Drogui, D. Robert, Photocatalytic oxidation of carbamazepine: application of an experimental design methodology, Water Air Soil Pollut. 227 (2016) 1–16.
[64] V. Vaiano, C.A. Jaramillo-Paez, M. Matarangolo, J.A. Navío, M.D.C. Hidalgo, UV and visible-light driven photocatalytic removal of caffeine using ZnO modified with different noble metals (Pt, Ag and Au), Mater. Res. Bull. 112 (2019) 251–260.
[65] R. Muangmora, K. Roongraung, P. Kemacheevakul, S. Chuangchote, Photocatalytic degradation of pharmaceuticals from water using nitrogen-doped titanium dioxide coated on fiberglass cloth, J. Clean. Prod. 397 (2023) 136487–136497.
[66] M.N. Chong, B. Jin, Photocatalytic treatment of high concentration carbamazepine in synthetic hospital wastewater, J. Hazard Mater. 199 (2012) 135–142.
[67] M.F. Atitar, A. Bouziani, R. Dillert, M. El Azzouzi, D.W. Bahnemann, Photocatalytic degradation of the herbicide imazapyr: do the initial degradation rates correlate with the adsorption kinetics and isotherms? Catal. Sci. Technol. 8 (2018) 985–995.
[68] C. Castañeda, J.J. Martínez, L. Santos, H. Rojas, S.M. Osman, R. Gómez, R. Luque, Caffeine photocatalytic degradation using composites of NiO/TiO_2–F and CuO/TiO_2–F under UV irradiation, Chemosphere 288 (2022) 132506–132514.
[69] R. Muangmora, P. Kemacheevakul, P. Punyapalakul, S. Chuangchote, Enhanced photocatalytic degradation of caffeine using titanium dioxide photocatalyst immobilized on circular glass sheets under ultraviolet C irradiation, Catalysts 10 (2020) 964–978.
[70] S. Raha, M. Ahmaruzzaman, Novel magnetically retrievable $In_2O_3/MoS_2/Fe_3O_4$ nanocomposite materials for enhanced photocatalytic performance, Sci. Rep. 11 (2021) 1–23.
[71] J. Suwanboriboon, W. Meesiri, W. Wongkokua, An application of spectrophotometer for ADMI color measurement, J. Phys. Conf. Ser. 1144 (2018), 012064.